Ternary chalcogenide Na_2MoSe_4 is a direct bandgap semiconductor*

Etienne I. Palos,† Armando Reyes-Serrato, Gabriel Alonso-Nuñez, and J. Guerrero Sánchez‡
Centro de Nanociencias y Nanotecnología,
Universidad Nacional Autónoma de México,
Apdo. Postal 14, 2280 Ensenada B.C., México

First-principles computations were performed on a set of hypothetical crystal structures to determine the ground state structure and electronic properties of the sodium molybdenum selenide Na_2MoSe_4. First, we approximate the ground state of the candidate structures through isotropic expansion. Formation enthalpy calculations reveal that the ground state structure of Na_2MoSe_4 is a simple orthorhombic *oP* lattice, with space group *Pnma*. We investigate the electronic structure of the *oP* structure as well as the metastable phases, showing semiconducting behaviour in three of them. Finally, we employ the Tran-Blaha modified Becke-Johnson exchange potential to model the electronic band structure of Na_2MoSe_4 and show that it is a direct bandgap semiconductor with a fundamental band gap at the Γ point. This is the first detailed analysis of the structure and properties of the semiconducting Na_2MoSe_4, an alkali transition metal chalcogenide that is isostructural to a set of known inorganic and hyrbrid organic/inorganic analogs whose physics have been until now overlooked, but display high promise for next generation optoelectronics and photovoltaics.

I. INTRODUCTION

A truly fascinating class of inorganic materials is the cherished family of transition metal chalcogenides (TMC). Its general composition is M-X, where M = transition metals (e.g. Mo, W, Re) and X = chalcogen anion (i.e. S, Se, Te) [1]. This broad family of presents extended structures (bulk) [1–3] and two-dimensional materials, with promising applications in next-generation technologies due to their broad spectra of physical and chemical properties [4–7]. Discoveries in TMC research have led to advances in our understanding of semiconductors, superconductors, topological insulators, ionic and mixed conductors, catalysts and photocatalysts [8–12] and recently an entirely exciting novel class of TMC-perovskites engineered for applications in optoelectronics and solar cells [13, 14].

Although the TMC family is large, its chemical space remains overwhelmingly unexplored when compared to transition metal oxides (TMO), with a ratio of roughly 2500 TMO to 450 TMCs [15]. Moreover, little is currently known about ternary transition metal selenides (TM-Se).

As members of the TMC family, TM-Se materials have increased in interest and have found applications within the realm of catalysis [16]. In 2005, Evans and coworkers demonstrated that solvothermal techniques are appropriate for the the synthesis of bulk ternary TM-Se. In their report, they discussed the chemistry of Cu_2MX_4, where M = W or Mo; X = S, Se, Se/S. Among these materials, Cu_2WSe_4 was identified as semiconductor [17].

Efforts are continuously made to explore the chemical space of TMCs. However, the discovery of QMX compounds, where Q = cation, M = transition metal and X = chalcogen anion, remains a challenge. This fact was highlighted in a recent computational and experimental investigation of TMCs, reporting the phase diagrams for twenty-four new structures. Although the materials are predicted to be stable, the synthesis of the compounds was rendered unsuccessful. [3].

The recent discovery of low dimensional ternary Na-Cu-Se materials by Kanatzidis and coworkers provides new insights into the chemistry of the A-TM-Se chemical space, where A is an alkali metal. We highlight the discovery of the layered metal $NaCu_6Se_4$ with mixed valency [18], the mixed-valent two-dimensional metal $NaCu_4Se_3$ [19] and the two-dimensional metal $NaCu_4Se_4$, which presents high hole mobility and giant magnetoresistence [20].

This leads us to think in general terms about the physics and applications of alkali-transition metal chalcogenides, AMX (A = alkali metal, M = transition metal, X = chalcogen). In a recent work by Z. Xia *et al*, it is discussed the chemistry of a new alakali-transition metal chalcogenide, $CsCu_5Se_3$. This ternary selenide is an *almost* direct bandgap semiconductor, with an $E_g = 1.04eV$. The material crystallizes in the *oP* lattice, in space group *Pmma* (No. 51) and it can be achieved via the solvothermal method. Authors also explored similar compounds to complete the family of materials by synthesizing and characterizing $CsCu_5S_3$ and proposing $CsCu_5Te_3$[21]. On another note, superconductivity has also been observed in narrow-gap semiconductors within the AMX family, $RbBi_{11/3}Te_6$ and $CsBi_4Te_6$ [22, 23]. Although a few (3) sodium molybdenum selenides can be found in the Materials Project and the ICSD [15] databases, none are semiconducting (See Supplemental

* Supplementary information available

† g5_palo16@ens.cnyn.unam.mx
‡ guerrero@cnyn.unam.mx

Information).

The combination of computational materials design and experiment will undoubtedly continue to accelerate catalysis and materials science [24]. Particularly, the availability of crystal exploration and prediction tools such as the web-based repository, The Materials Project [25] and crystal structure prediction packages such as CALYPSO [26, 27] and XtalOpt [28, 29] are key for materials discovery and bottom-up design [30–34]. As these techniques become robust, they become accepted by the broader community as an standard for materials design.

The traditional or go-to route in materials design consists of "manual" solid substitution (ionic or interstitial) of a known and analogous material. In this work, our objective is to model and determine the ground state structure for Na_2MoSe_4 to then investigate its electronic structure. In this sense, it might be wise to take the stable and clearly chemically similar Na_2MoO_4 (face centered cubic (cF), substitute our chalcogen anion and find the ground state. Another lesser obvious possibility would be to part from the relative Rb_2WS_4 (primitive orthorhombic (oP)) by substituting K^+ for Na^+, W^+ for Mo^+, S^- for Se^- and find the ground state. Which would be a better choice? One route (i.e. case the structure's symmetry) will lead us to the ground state and the other must lead towards instability. From the *a priori* postulate of statistical thermodynamics, before we calculate anything, the probability of these structures being the energetically favored is exactly the same for both routes.

In brief, we employ a materials prediction method combined with Kohn-Sham density functional theory to model and characterize the sodium molybdenum selenide structure, Na_2MoSe_4. We generate a pool of candidate structures, set criteria to quickly screen our candidates based on symmetry and stoichiometry, and determine the energetically favored candidate through first-principles thermodynamics. Finally, we focus on the electronic structure of the ground state structure.

II. CRYSTAL STRUCTURE PREDICTION

To address the issue of structure determination, we followed the crystal structure prediction method of Hautier *et al* [35] based on data mined ionic substitutions. It has been demonstrated that the method of data mined ionic substitutions can generate likely crystal structures at a fraction of the computational cost of evolutionary algorithms [3], due to the fact that the substitutions are generated posterior to the analysis of existing crystal structures listed in the ICSD. For the reader's convenience, we briefly outline the data mining + ionic substitution (DM+IS) methodology:

(i) Systems of ions X_i $(i = 1, 2, 3, ..., n)$ are represented as a component vectors of n elements,

$$\mathbf{X} = (X_1, X_2, X_3, ..., X_n). \tag{1}$$

(ii) Once a given number of candidate structures is generated, the probability function P_n for two compounds existing in the same crystal structure is expressed as

$$P_n(\mathbf{X}, \mathbf{X'}) = P_n(X_1, ..., X_1', ..., X_n'). \tag{2}$$

(iii) p_n is approximated by using the feature function $f(\mathbf{X},\ \mathbf{X'})$,

$$P_n(\mathbf{X},\ \mathbf{X'}) \approx \frac{\exp[\sum_i \lambda_i f_i(\mathbf{X},\mathbf{X'})]}{\Xi} \tag{3}$$

(iv) In equation (3), Ξ is analogous to a partition function that ensures normalization of P_n, and λ_i is the weight corresponding to $f_i(\mathbf{X},\mathbf{X'})$. It is noteworthy that only binary feature functions $f_i(\mathbf{X},\mathbf{X'})$ are assigned to pairs of ions (α, β),

$$f_k^{\alpha,\beta}(\mathbf{X},\mathbf{X'}) = \begin{cases} 1, & X_k = \alpha, X_k' = \beta. \\ 0, & else. \end{cases} \tag{4}$$

(v) The likelihood of the binary α to β substitution is determined by λ_i, obtained from ionic compounds in the ICSD. For a detailed description of DM+IS method and its reach, we refer the reader to the paper by Ceder and coworkers [35].

Here, our DM+IS search generated over sixty-five hypothetical sodium molybdenum selenide structures, of which twenty-one present our hypothesized stoichiometry. The list of Na_2MoSe_4 candidates is found in Table S1 and it has been made public in the Materials Project Database [25]. The four candidates with highest likelihood of existing in their predicted space groups were analyzed in this work.

III. FIRST-PRINCIPLES COMPUTATIONS

Our first-principles computations based on Kohn-Sham Density Functional Theory (DFT) were carried out primarily using the plane-wave pseudo-potential method implemented in Quantum ESPRESSO [36, 37]. We employ the General Gradient Approximation (GGA) functional with corrected-for-solids Perdew-Burke-Ernzerhof (PBEsol) parametrization for the exchange correlation potential [38], as it has been shown that the PBEsol is better suited to approximate lattice constants and surface energies when compared to PBE and LDA [39–41]. The ground state structures were determined by varying the volume isotropically, to control symmetry while fully relaxing atomic positions under a tolerance of 13.605×10^{-5} eV/atom for total energy and net forces of 0.025 eV·Å^{-1} per atom. These computations were performed using ultrasoft pseudopotentials (USP) with a plane-wave kinetic energy cutoff of 40 Ry (544 eV), charge density cutoff f of 320 Ry (4,354 eV) and a convergence threshold of 1×10^{-8} eV for self-consistency. Monkhorst-Pack Γ-centered integration grids were used to sample the first Brillouin Zone [42]. For structural

optimization computations of the cF, oF, oP and mC phases, integration grids of $6\times6\times4$, $8\times6\times5$, $6\times8\times4$, $5\times5\times4$ were used. To model the electronic structure we then increased the density of the k-points integration grids to $24\times28\times20$ (cF), $32\times24\times20$ (oF), $24\times32\times18$ (oP) and $30\times30\times24$ (mC). The USP used in all pw-DFT computations were generated with the following valence configurations: Na ($2s^1$, $3s^2$, $2p^2$), Mo ($4s^1$, $5s^2$, $5p^2$, $4d^5$) and Se ($4s^1$, $4p^2$, $3d^3$) [43].

It is well known GGA fails to predict the fundamental bandgap of semiconductors. Therefore, we correct the electronic band structure of the favored phase by performing meta GGA (MGGA) calculations using the Trahn-Blaha modified Becke-Johnson (TB-mBJ) exchange potential [44]. In order to obtain optimal results, our TB-mBJ computations were carried out in the framework of the Augmetnted Planewave plus Local Orbital (APW+lo) method as implemented in the all-electron code Wien2k[45].

IV. CANDIDATE STRUCTURES

We consider the following four candidate structures of Na_2MoSe_4: a face centered cubic (cF) phase with space group *Fd-3m* (227), a face centered orthorhombic (oF) with space group *Fddd* (70), a primitive orthorhombic (oP) with space group *Pnma* (62) and a base centered monoclinic (mC) with space group *C2/m* (12). The unit cells are sketched in Figure 1 (a)-(d). The structural details for the evaluated systems are shown in Table 1, which includes the raw (generated) DM+IS and the computed (equilibrium) parameters. From the obtained results it is clear that the equilibrium volume changes significantly with respect to the DM+IS volume, with the exception of the oP structure. For example, $\Delta V^{oP} = 2\%$ versus $\Delta V^{cF} = 26\%$. Since we have unit cells with different number of atoms, to formally asses which of the candidates is the favored ground state phase of Na_2MoSe_4, we proceed to calculate the molar formation enthalpy $\Delta H^s_{f(AMX)}$. It reads

$$\Delta H^s_{f(AMX)} = U^s_{(AMX)} - \sum_i N_i \mu^s_i, \qquad (5)$$

where $U^s_{(AMX)}$ is the total energy of disodium tetraselemolybdate in solid phase, N_i is the number of atoms of a constituent i with chemical potential μ_i in solid phase. This is, $2\mu^s_{Na}$, μ^s_{Mo} and $4\mu^s_{Se}$. The chemical potentials μ for the constituent species were calculated based on DFT energies of their equilibrium crystal structures under the same relaxation criteria and convergence thresholds as the Na_2MoSe_4 candidates. Additionally, the energetics analysis was cross-checked, fully relaxing all candidate structures at the PBE level. No significant changes on the lattice parameters were found. The values for $\Delta H^s_{f(AMX)}$ are shown in Table 2. Note that oP is the favored phase of the selenide with ΔH^s_f values

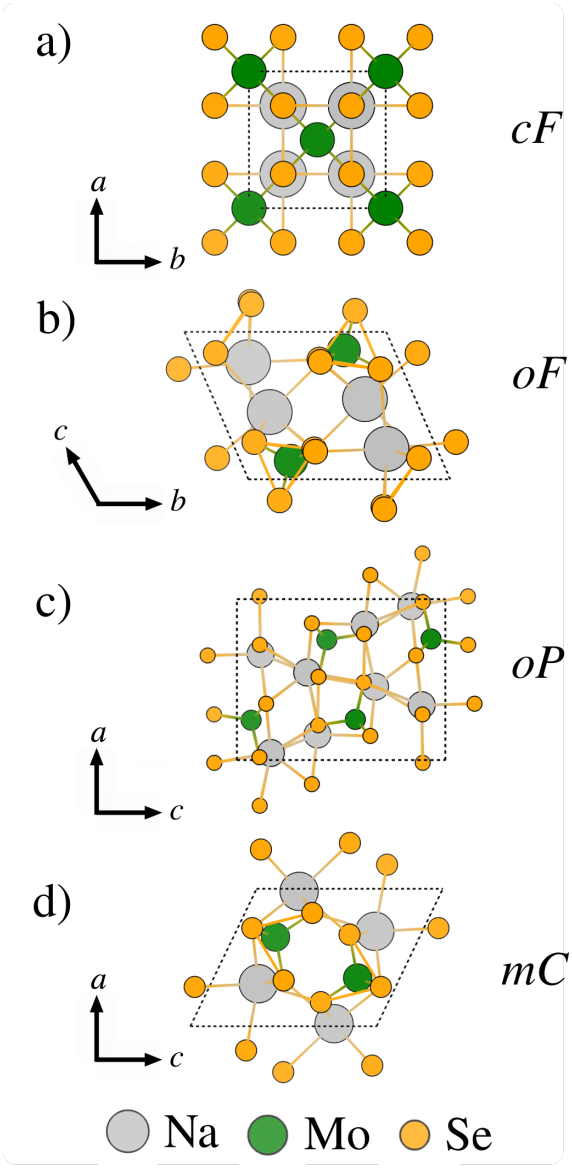

FIG. 1. Sketch of the candidate structure unit cells under this study for Na_2MoSe_4. The candidates are labeled by their lattice type (a) face centered cubic cF, (b) face centered orthorhombic oF, (c) simple orthorhombic oP and (d) base centered monoclinic mC. The colors corresponding to Na, Mo and Se are grey, green and orange respectively.

of -5.14 (PBEsol) and -5.11 (PBE) eV per formula unit (eV/f.u.). We find these relative formation enthalpies to be in good agreement, as the relative error between the PBE/PBEsol calculations is less than 2% for all phases with the exception of the least stable cF, in which a larger discrepancy is observed. We encourage further studies to calculate the phonon band structure for the meta-stable phases, as we recognize the importance of these calculations to assess its dynamical stability. Here, our scope is to determine the most energetically stable structure for the already synthesized Na_2MoSe_4 compound[46, 47], and calculate its electronic properties. Once determined

TABLE I. Predicted and optimized lattice parameters for the Na_2MoSe_4 candidate structures computed at the GGA-(PBEsol) level of theory.

System	**a** (Å)	**b** (Å)	**c** (Å)	V (Å^3)	α	β	γ
cF: *Fd-3m* (227)							
DM+IS	6.44	6.44	9.11	188.89	45	45	90
This work	8.14	8.14	11.51	238.76	45	45	90
oF: *Fddd* (70)							
DM+IS	6.31	8.39	10.85	223.77	130	149	56
This work	7.71	10.24	13.26	273.38	130	149	56
oP: *Pnma* (62)							
DM+IS	9.32	6.84	12.08	770.49	90	90	90
This work	9.12	6.69	11.81	753.92	90	90	90
mC: *C2/m* (12)							
DM+IS	6.88	6.08	7.54	254.92	90	67	63
This work	7.78	6.88	8.52	368.58	90	67	63

TABLE II. Formation enthalpies ΔH_f for Na_2MoSe_4 candidate structures calculated from GGA(PBEsol) and GGA(PBE) computations. ΔH_f si shown in eV per formula unit (eV/f.u.) and eV/atom.

System	ΔH_f (eV/f.u.)	ΔH_f (eV/atom)
cF		
PBEsol	-4.39	-0.63
PBE	-4.02	-0.57
oF		
PBEsol	-4.90	-0.70
PBE	-4.83	-0.69
oP		
PBEsol	-5.14	-0.73
PBE	-5.11	-0.73
mC		
PBEsol	-5.03	-0.72
PBE	-4.91	-0.70

the most stable phase, from this point forward, we focus our attention only to the *oP* phase with *Pnma* space group. To further cross check the ground state of the *Pnma* candidate, we take the initial (DM+IS) structure and optimize it at the APW+lo/PBEsol level of theory. The volume V is varied isotropically. The equilibrium volume is obtained using the Birch-Murnaghan equation of state (BM-EOS), given by

$$E(V) = E(V_0) + \frac{B_0 V}{B_0'}\left[1 + \frac{(V_0/V)^{B_0'}}{B_0' - 1}\right] \qquad (6)$$

where V_0 is the predicted equilibrium volume, and B_0, B_0' are the bulk modulus and its pressure derivative respectively. The ground lattice parameter is $a = 9.21$ Å, which is in fine agreement with our pw(pseudo-potential) computed lattice constant $a = 9.12$, with an absolute error $e_a =\leq 1\%$. At V_0, the bulk modulus for Na_2MoSe_4 is $B_0 = 56.07$ GPa with a numerical derivative of $B_0' = 4.41$.

Due to the fact that the hypothetical crystal structures were generated from chemical analogs, it is reasonable to infer that the true equilibrium structure of our material (*oP*) should result isostructural to other materials governed by same chemical principles (e.g. valency, electronegativity, position within the periodic table etc.). Furthermore, it is said that compounds governed by the same chemical principles as Na_2MoSe_4 will also be favored in the *oP* lattice. This is in fact the reasoning and strength behind probabilistic models for crystal structure prediction. Therefore, the probability P of a material to exist in a specific crystal system (e.g. *oP* (*Pnma*)) will be influenced by the size of the known isostructural family[35, 48–50]. To elucidate, we match our evaluated structures to their analogs. First, we found our least stable candidate $cF(Fd-3m)$ to be isostructural to the stable phase of Na_2MoO_4 [ICSD No. 44523]. The metastable phase of Na_2MoO_4 [ICSD No. 151971] is characterized by the *Fddd* space group and isotructural to our *oF* candidate. The *mC* candidate is isostructural to the molecular crystal K_2MoO_4 [ICSD No. 16154]. Lastly, our most stable *oP* phase is isostructural to (or based on) K_2MoS_4 [ICSD No. 409563]. Notably, the following isostructures have been synthesized: Na_2MoSe_4 with $oP(Pnma)$ symmetry: K_2MoS_4, Cs_2MoSe_4, Rb_2MoSe_4, , Cs_2MoS_4, Rb_2MoS_4, K_2WSe_4 and Rb_2WS_4 [51–55] and could potentially be intrinsic semiconductors. Additionally, hybrid organic/inorganic members of the family R_2MX_4 (e.g. R = CH_3NH_3 ; M = Mo,W ; X = S, Se) have also been reported [56, 57]. Note, throughout the A_2/R_2MX_4 family, X is either S or Se. To the best of our knowledge, no detailed theoretical studies of these materials are available in the literature. Given the electronic structure of Na_2MoSe_4 (see section VI), it results of interest to the broader community to understand the physics and chemistry of the *oP* A/R_2MX_4 compounds and their potential applications. Hence, we intend for our work to serve as a primer for future theoretical and experimental studies on the structural and electronic properties of both the inorganic and hybrid organic/inorganic analogs of Na_2MoSe_4.

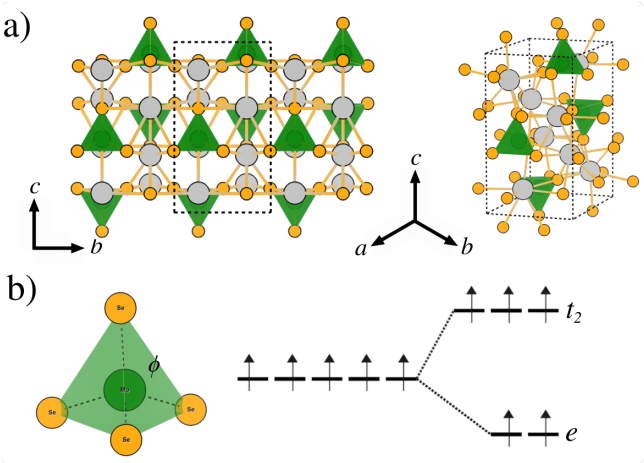

FIG. 2. Illustration of (a) isometric and front views of oP ($Pnma$) phase of Na_2MoSe_4 and (b) the $[MoSe_4]^-$ tetrahedron with a schematic illustration of the tetrahedral crystal field that splits the Mo $4d_5$ orbitals into two groups, namely t_2 and e. As seen in (a) Na^+ ions are intercalated through the $MoSe_4$ tetrahedral layers.

V. STRUCTURE AND SYMMETRY OF ORTHORHOMBIC SODIUM MOLYBDENUM SELENIDE

The disodium tetraselemolybdate, which can be written as $Na_2[MoSe_4]$, is a molecular crystal is favored to grow in the simple orthorhombic (oP) crystal system with space group $Pnma$ (No. 62), as shown in Figure 2. It has inversion symmetry, and is can be defined by eight symmetry operations. In Figure 2-a, an illustration of the frontal and isometric views are shown. The Na_2MoSe_4 structure is three-dimensional, (i.e. there are no van der Waals layers) with two equivalent Na^{1+} sites. Note that Mo^{6+} is in tetrahedral coordination τ_4 (i.e. $\tau_4 = 1$), bonded to four Se^{2-}atoms at each vertex. There is no Mo-Na bond, and the Na cations are intercalated throughout the lattice. This promotes the one-dimensional (directional) growth of the $[MoSe_4]$ tetrahedrons. Additionally, the electronic charge of Na induces a distortion in the tetrahedron (distortion index $t_4^{'} = 0.006$) yielding a slightly elongated Mo-Se bond ($d = 2.33$ Å) versus the other three ($d = 2.30$ Å), and a broadening of Se-Mo-Se bond angle ϕ from $\phi = 109.55°$ to $\phi = 115°$ as shown in Figure 2-b. The average Mo-Se bond length is $\bar{l} = 2.31$ Å. This distortion is caused by electronic charge effects of a Na^{1+} atom in proximity to one Se vertex ($r = 2.98$ Å. The distortion can be also measured by the tetrahedron edges, conformed by Se-Se inter-atomic distances. The tetrahedron edge lengths are $l = 3.778$, 3.576 and 3.793 Åsrespectively. The omitted length values are redundant in nature. A spread of Na-Se bond distances can be found in the two Na sites, with values ranging between 2.98 3.48 Å. In one Na^{1+} site, Na^{1+} is bonded in a 8-coordinate geometry to eight Se^{2-} atoms. In the other, our sodium cation is bonded in a 9-coordinate geometry to 9 Se anions. There are three nonequivalent Se^{2-} sites. In the first Se site, Se^{2-} is bonded in a single coordinate geometry to four Na^{1+} and one Mo^{6+} atom. In the second site, Se^{2-} is bonded in a 6-coordinate geometry to five Na^{1+} and one Mo^{6+} atom. In the third Se site, Se^{2-} is bonded in a 5-coordinate geometry to four Na^{1+} and one Mo6+ atom. Our structural analysis is in agreement with the available information for its reported analogs [51–55]. Note, the intercalation of Na atoms could favor an energetically low-cost substitution (or displacement) of cations, enabling the tunability of these materials' properties.

VI. ELECTRONIC STRUCTURE

The electronic structure of all candidates was investigated. We show in Figure 3 the electronic band structure of the candidate phases of Na_2MoSe_4 and their corresponding total density of states (DOS). Conventional k paths were used [58, 59]. In all plots, the Fermi energy E_F is set to zero. From the band structure plots, it is clear that one of four phases is metallic; cF (Figure 3(a)), where the Density of States (DOS) plot shows the typical electronic structure of a metal. The remaining three (less symmetric) are intrinsic semiconductors. The oF phase is a direct bandgap semicondutor (Figure 3 (b)), with a bandgap $E_g = 0.62$ eV at Γ, while the mC phase is an indirect bandgap semiconductor with $E_g = 0.45eV$ running from $A - \Gamma$ (Figure 3(d)). Total DOS is shown depicting the corresponding semiconducting characteristics. Lastly, our GGA calculations show that oP Na_2MoSe_4 has a fundamental bandgap of $E_g(GGA) = 0.24$ eV at Γ (Figure 3 (c)). Since the oP structure is energetically favored, we focus only on this phase from here in and shall refer to this phase simply as "Na_2MoSe_4".

In order to better understand the electronic band structure of Na_2MoSe_4, we adopt an alternative k path from the work of Xia *et al*[21] on oP $CsCu_5Se_3$. At this point, we analyze nature of the Na_2MoSe_4 band structure. Let us recall that the Mo is in coordination τ_4 with Se atoms at each vertex. Given the electronic nature of our species, it is inferred that the valence bands that contribute to the Fermi level E_F are composed of Mo d orbitals, with mild hybridization from the Se p orbitals. Therefore, it can be said that the electronic (semiconducting) properties of the material arise mainly from the $[MoSe_4]$ sub-unit and that the effects of Na s, p electrons are negligible. However, although Na doesn't seem have influence on the band structure of the selenide, it is reasonable to believe that the displacement of Na throughout the lattice (diffusion) or its substitution to another ion (or molecule) could have an effect on the value of E_g.

We further investigate the τ_4 sub-unit by treating the Se atoms as point charges around the Mo central ion, to study their bonding strength in terms of Coulombic interactions. In this sense, Crystal Field Theory (CFT) qual-

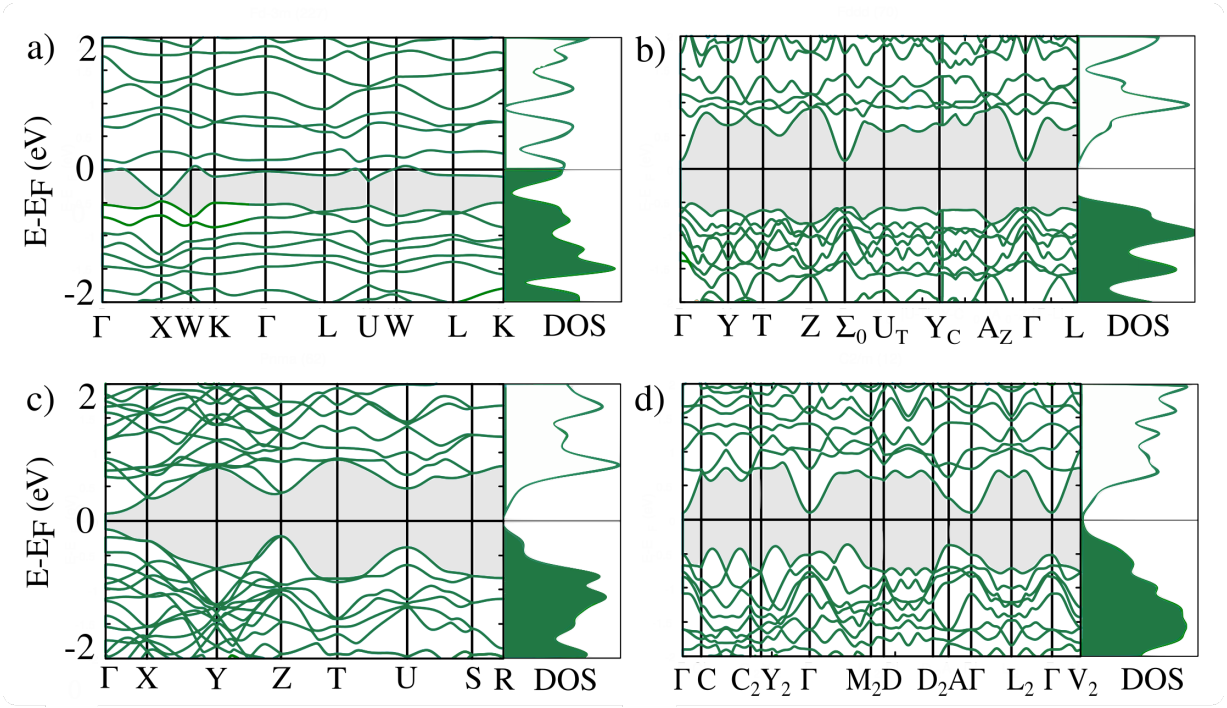

FIG. 3. The electronic band structure and total density of states is shown for the (a) cF, (b) oF, (c) oP and (d) mC candidate phases of Na_2MoSe_4. The Fermi energy E_F is set to 0.

itatively predicts how the electrons in the Mo $4d$ orbitals respond to the effective electrostatic potential imposed by its neighboring Se atoms. In t_4, the initial five-fold degeneracy of the $4d$ orbitals will break. This will give rise to the the orbital groups t_2 orbitals (d_{xy}, d_{yz}, d_{yz}) and the e orbitals $(d_{x^2-y^2}, d_{z^2})$. A schematic illustration of an idealized τ_4 CF is shown in the right hand side of Figure 2(b). Let us recall the electronic configuration for Mo, $[Kr]4d_5 5s_1$, to see that there is only one (unpaired) electron occupying each d orbital. This conformation is energetically much more stable than if we were to occupy the orbitals in such a way that we have paired electrons. As a consequence, this along with weak overlap between the Mo d and Se p orbitals leads to high-spin behaviour. In essence, Na_2MoSe_4 is paramagnetic with a potentially large Fermi velocity v_F. Also note, that the qualitative CFT analysis indicates that spin orbit coupling (SOC) effects are weak [60] in Na_2MoSe_4. In figure 4, we elucidate on this by plotting the GGA and GGA+SOC band structures along the $\Gamma-X-U-\Gamma-Y-T-\Gamma-Z-S-R$ k-path. The FBZ is shown in Figure 4 (b). Here, we refer to the band structure simply as GGA as PBE and PBEsol, having the same form of correlation-exchange, yield the same band structure. For completeness, we also plot the band structure by introducing an empirical Hubbard potential (GGA+U ; $U = U_{eff} = 3.5$ eV [31]) to test for Coulomb effects in Mo d electrons (see Supplementary Information). As expected, no change was observed in E_g upon calculating the band structure with SOC or U_{eff}.

Note, in Figure 4(a) that the effect of SOC, Δ_{SOC}, is negligible and does not open/widen E_g. Note also, the band structure of Na_2MoSe_4 is highly isotropic. Note also,that the conduction band minimum (CBM) and valence band maxium (VBM) are mainly composed of Mo d and Se p. The dispersion of $E(k)$ near Γ is linear in regions $U \rightarrow \Gamma$, $\Gamma \rightarrow Y$, with clear parabolic topology at the VBM and CBM. In this region, $U \rightarrow \Gamma \rightarrow Y$, the electron and hole effective masses m_h^*, m_e^* and are expected to be constant. Therefore, there could potentially be high mobility transport within Na_2MoSe_4.

In Figure 5, the projected DOS (pDOS) is shown from $-2 \leq E_F \leq 2$ eV for the atomic contributions, Mo d, Se p and Na s electrons. Clearly the Na s states do not contribute near the Fermi level, and the hybridized d/p orbitals; Mo d states which (note $0 \leq E_F \leq 2$ eV) and the Se p states (note $-2 \leq E_F \leq 0$ eV) are the ones dominating the contributions around the Fermi level. We then decompose the contribution of summed Mo d into its constituent atomic orbitals in Figure 6 ; $d_{z^2}, d_{zx}, d_{zy}, d_{x^2-y^2}, d_{xy}$. Note that higher pDOS is observed above the Fermi level, due to the unoccupied states in the shells.

Although ground state GGA calculations can provide a reasonable first approximation to model the electronic structure of a material, it fails to predict the fundamental value of E_g. To be precise, GGA underestimates the bandgap. Hence, a precise approach such as the use of MGGA, hybrid funtional (e.g. HSE06 [61]) or the many-body perturbation theory method GW is desired. To achieve a predictive level, we have opted for the MGGA,

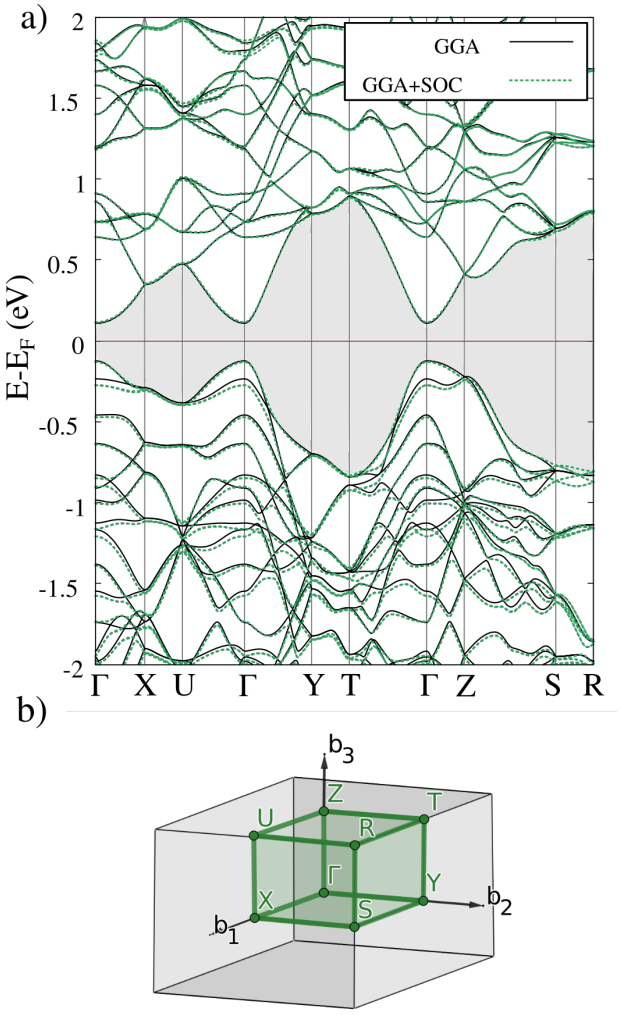

FIG. 4. Electronic band structure is shown in (a) modeled at the GGA (black - solid) and GGA+SOC (green - dashed) levels. The irreducible Brillouin zone and k-path for the oP lattice is shown in (b).

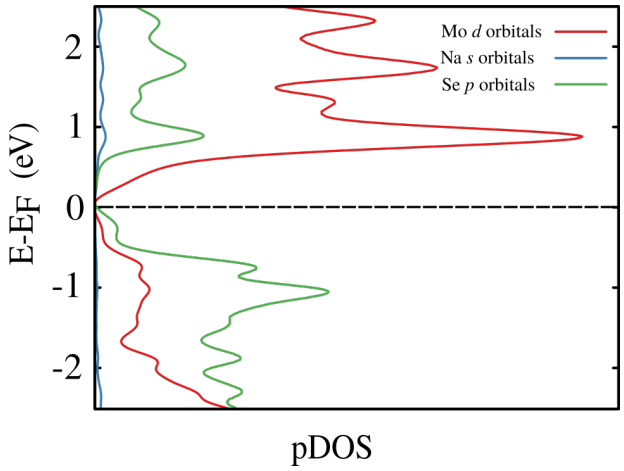

FIG. 5. Projected density of states is shown for the valence orbitals of each species.

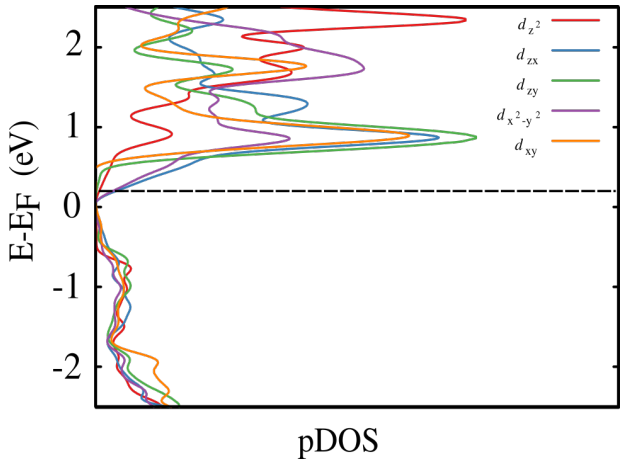

FIG. 6. Projected density of states is decomposed to show individual Mo d orbital contributions.

Trahn-Blaha modified version of the Becke-Johnson potential (TB-mBJ), designed and proven to yield robust results and comparable to HSE06, *GW* and experimental results, when used with a APW+lo basis set at a fraction of the computational cost [44, 62–67]. In the present scenario, the use of TB-mBJ is considered adequate as no further corrections for correlation or spin-orbit coupling are are needed.

The TB-mBJ exchange potential reads

$$\mathbf{v}_{x,\sigma}^{TB-mBJ}(\mathbf{r}) = c\mathbf{v}_{x,\sigma}^{BR}(\mathbf{r}) + (3c-2)\frac{1}{\pi}\sqrt{\frac{5}{12}}\sqrt{\frac{2t_\sigma(\mathbf{r})}{\rho_\sigma(\mathbf{r})}} \quad (7)$$

where ρ_σ is the electronic density, t_σ is the kinetic energy density and $\mathbf{v}_{x,\sigma}^{BR}(\mathbf{r})$ is the Becke-Roussel potential[68]. Additionally, since it was shown that correlation does not play an important role in the band structure of Na_2MoSe_4, not affecting the band topology or changing E_g, a MGGA approach that corrects exchange is appropriate. Our TB-mBJ calculation of the band structure yields the same band topology an a bandgap of $E_g^{TB-mBJ} = 0.53$ eV at the Γ point. This is shown in figure 6. One would expect to obtain of $E_g = 0.53 \pm 0.02$ eV from HSE06, as TB-mBJ has been shown to perform at the same level of accuracy as HSE06 when treating semiconductors, both with a standard deviation of the relative error $\sigma = 22\%$ within the APW+lo framework. Additionally, Tran and Blaha demonstrate that as the E_g increases, TB-mBJ yields better performance than HSE06 when compared to the experimental data [69]. Thus, one can calculate the bandgap E_g of large and complex systems at a predictive level. Therefore, a MGGA TB-mBJ should faithfully reproduce the physics of the inorganic A_2MX_4 and hybrid organic/inorganic R_2MX_4, with 84 atoms in the unit cell. This has recently been achieved and for complex semiconducting materials structures such as inorganic organic/inorganic perovskites [70, 71], serving as motivation for complete

description of the aforementioned *oP* compounds. Although the bandgap isn't yet "ideal" for applications in traditional optoelectronic devices or photovoltaics, Na_2MoSe_4 with an instrinsic direct bandgap of 0.53 eV holds potential for applications in infrared optoelectronics and high-speed electronic heterostructures and devices. Keeping in mind, the bandgap is tunable via ionic displacement and/or substitution. Hence, it is of interest to investigate (i) the electronic structure of the A_2MX_4 (R_2MX_4) and (ii) the effects of Na-displacement throughout the lattice. This can be achieved, for example, through nudge-elastic band DFT calculations[72].

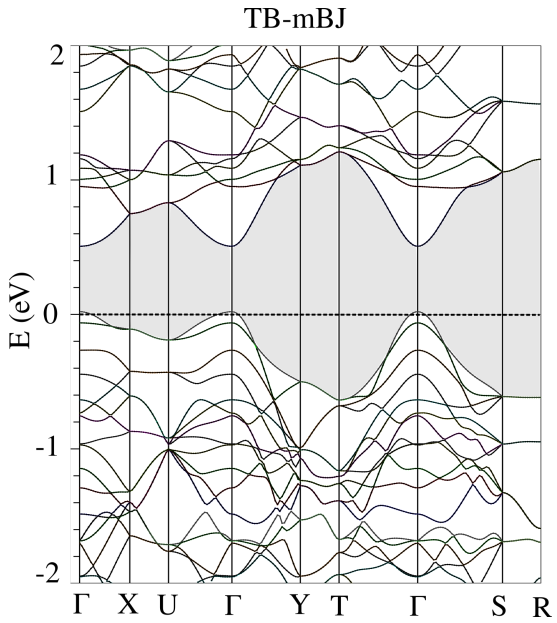

FIG. 7. Electronic band structure of Na_2MoSe_4 corrected by TB-mBJ. Here, the VBM is set to zero. Note that the band topology is preserved when compared to GGA.

VII. SUMMARY AND CONCLUSIONS

In summary, the ground state structure and electronic properties of the Na_2MoSe_4 structures were theoretically investigated. First-principles computations were performed on four candidate structures generated through ionic substitution. Namely, face centered cubic, face centered orthorhombic, simple orthorhombic and base centered monoclinic. The stability analysis reveals that the simple orthorhombic is the favored phase, with space group *Pnma*. Additionally, the electronic band structure depicts semiconducting behaviour for all candidates with an exception of the cubic phase. Finally, the band structure of orthorhombic Na_2MoSe_4 is modeled through MGGA computations based on the Trahn-Blaha modified Becke-Johnson exchange potential, yielding a direct fundamental bandgap of 0.53 eV at Γ. Thus, this bandgap is suitable Na_2MoSe_4 for applications in infrared optoelectronics and high speed electronics. The valence and conduction bands near the Fermi level are composed of Mo *d* and Se *p* orbitals, although it is expected that substitution or diffusion of the alkali-metal cation could pose an effect on the band structure. Additionally, due to its structure, it is expected that Na_2MoSe_4 could be classified as a mixed conductor, applicable in Na-ion batteries. Our analysis indicates that the general physics of Na_2MoSe_4 is transferable to *oP* chemical analogs. By disclosing the crystal and electronic band structure of disodium molybdenum selenide, we also shine light onto the potential of related compounds. Lastly, this work is a major first step towards a fundamental understanding and application of alkali-metal transition metal chalcogenides and hybrid organic/inorganic transition metal chalcogenide semiconductors.

ACKNOWLEDGMENTS

We thank DGAPA-UNAM projects IA100920 and IG200320 for partial financial support. Calculations were performed in the DGCTIC-UNAM Supercomputing Center, project LANCAD-UNAM-DGTIC-390 and Laboratorio Nacional de Supercmputo del Sureste de Mxico, CONACYT member of the network of national laboratories. J.G.S acknowledges THUBAT KAAL IPICYT supercomputing center for computational resources. E.I.P acknowledges financial support from CONACyT for a SNI-III assistantship under G.A.N. E.I.P thanks Roald Hoffmann (Cornell) for insightful conversations on materials prediction.

[1] F. Jellinek, Transition metal chalcogenides. relationship between chemical composition, crystal structure and physical properties, Reactivity of Solids **5**, 323 (1988).
[2] F. Lopez-Vergara, A. Galdamez, V. Manriquez, P. Barahona, and O. Pena, Magnetic properties and crystal structure of solidsolution cu2mnxfe1xsns4 chalcogenides with stannitetype structure, Physica Status Solidi B **251**, 323 (2014).
[3] A. Narayan, A. Bhutani, S. Rubeck, J. N. Eckstein, D. P. Shoemaker, and L. K. Wagner, Computational and experimental investigation for new transition metal selenides and sulfides: The importance of experimental verification for stability, Phys. Rev. B **94**, 045105 (2016).
[4] J. Panand Q. Yan, 2d transition metal dichalcogenides, Nature Reviews Materials **2**, 17033 (2017).
[5] Z. Hu, Z. Wu, C. Han, J. He, Z. Ni, and W. Chen, Two-dimensional transition metal dichalcogenides: interface

and defect engineering, Chem. Soc. Rev **47**, 3100 (2018).
[6] T. D. Thanh, N. D. Chuong, H. V. Hien, T. Kshetri, L. H. Tuan, N. H. Kim, and J. H. Lee, Recent advances in two-dimensional transition metal dichalcogenides-graphene heterostructured materials for electrochemical applications, Progress in Materials Science **96**, 51 (2018).
[7] W. Choi, N. Choudhary, G. H. Han, J. Park, D. Akinwande, and Y. H. Lee, Recent development of two-dimensional transition metal dichalcogenides and their applications, **96**, 116 (2017).
[8] S. M. Kwon, J. K. Won, J.-W. Jo, J. Kim, H.-J. Kim, H.-I. Kwon, J. Kim, S. Ahn, Y.-H. Kim, M.-J. Lee, H. ik Lee, T. J. Marks, M.-G. Kim, and S. K. Park, High-performance and scalable metal-chalcogenide semiconductors and devices via chalco-gel routes, Science Advances **4**, 9104 (2018).
[9] Y.-T. Hsu, A. Vaezi, M. H. Fischer, and E.-A. Kim, Topological superconductivity in monolayer transition metal dichalcogenides, Nature Communications **8**, 14985 (2017).
[10] A. West, Heterogeneous catalysis: No metal is an island, Nature Reviews CHemistry **2**, 0141 (2018).
[11] A. P. Tiwari, T. G. Novak, X. Bu, J. C. Ho, and S. Jeon, Layered ternary and quaternary transition metal chalcogenide based catalysts for water splitting, Catalysts **8**, 551 (2018).
[12] V. Agarwaland K. Chatterjee, Recent advances in the field of transition metal dichalcogenides for biomedical applications, Nanoscale **10**, 16365 (2018).
[13] A. Swarnkar, W. J. Mir, R. Chakraborty, M. Jagadeeswararao, T. Sheikh, and A. Nag, Are chalcogenide perovskites an emerging class of semiconductors for optoelectronic properties and solar cell?, Chem. Mater. **31**, 565 (2019).
[14] Q. Sun, H. Chen, and W.-J. Yin, Do chalcogenide double perovskites work as solar cell absorbers: A first-principles study, Chem. Mater. **31**, 244 (2019).
[15] A. Belsky, M. Hellenbrand, V. Karen, and P. Luksch, New developments in the inorganic crystal structure database (icsd): accesibility in support of materials research and design, Acta Crystallographica **58**, 364 (2002).
[16] J. Masud, W. P. Liyanage, X. Cao, A. Saxena, and M. Nath, Copper selenides as high-efficiency electrocatalysts for oxygen evolution reaction, ACS Appl. Energy Mater. **1**, 4075 (2018).
[17] C. J. Crossland, P. J. Hickey, and J. S. O. Evans, The synthesis and characterisation of cu2mx4 (m = w or mo; x = s, se or s/se) materials prepared by a solvothermal method, J. Mater. Chem. **15**, 3452 (2005).
[18] M. Sturza, C. D. Malliakas, D. E. Burgaris, F. Han, D. Y. Chung, and M. G. Kanatzidis, Nacu6se4: A layered compound with mixed valency and metallic properties, Inorg. Chem. **53**, 12191 (2014).
[19] M. Sturza, D. E. Burgaris, C. D. Malliakas, F. Han, D. Y. Chung, and M. G. Kanatzidis, Mixed-valent nacu4se3: A two-dimensional metal, Inorg. Chem. **55**, 4884 (2016).
[20] H. Chen, J. N. B. Rodrigues, A. J. E. Rettie, T.-B. Song, D. G. Chica, X. Su, J.-K. Bao, D. Y. Chung, W.-K. Kwok, L. K. Wagner, and M. G. Kanatzidis, High hole mobility and nonsaturating giant magnetoresistance in the new 2d metal nacu4se4 synthesized by a unique pathway, J. Am. Chem. Soc. **141**, 635 (2019).
[21] Z. Xia, H. Fang, X. Zhang, M. S. Molokeev, R. Gautier, Q. Yan, S.-H. Wei, and K. R. Poeppelmeier, Cscu5se3: A copper-rich ternary chalcogenide semiconductor with nearly direct band gap for photovoltaic application, Chemistry of Materials **30**, 1121 (2018), https://doi.org/10.1021/acs.chemmater.7b05104.
[22] C. D. Malliakas, D. Y. Chung, H. Claus, and M. G. Kanatzidis, Superconductivity in the narrow-gap semiconductor rbbi$_{11/3}$te$_6$, J. Am. Chem. Soc **138**, 14694 (2016).
[23] H. Chen, H. Claus, J.-K. Bao, C. C. Stoumpos, D. Y. Chung, W.-K. Kwok, and M. G. Kanatzidis, Superconductivity and structural conversion with na and k doping of the narrow-gap semiconductor csbi$_4$te$_6$, Chem. Mater **30**, 5293 (2018).
[24] J. Greeley, Theoretical heterogeneous catalysis: Scaling relationships and computational catalyst design, Annual Review of Chemical and Biomolecular Engineering **7**, 605 (2016).
[25] A. Jain, S. P. Ong, G. Hautier, W. Chen, W. D. Richards, S. Dacek, S. Cholia, D. Gunter, D. Skinner, G. Ceder, and K. a. Persson, The Materials Project: A materials genome approach to accelerating materials innovation, APL Materials **1**, 011002 (2013).
[26] Y. Wang, J. Lv, L. Zhu, and Y. Ma, Crystal structure prediction via particle-swarm optimization, Phys. Rev. B **82**, 094116 (2010).
[27] Y. Wang, J. Lv, L. Zhu, S. Lu, K. Yin, Q. Li, H. Wang, L. Zhang, and Y. Ma, Materials discovery via calypso methodology, Journal of Physics: Condensed Matter **27**, 203203 (2015).
[28] D. C. Lonieand E. Zurek, Xtalopt: An open-source evolutionary algorithm for crystal structure prediction, Computer Physics Communications **182**, 372 (2011).
[29] P. Avery, Z. Falls, and E. Zurek, Xtalopt version r11: An open-source evolutionary algorithm for crystal structure prediction, Computer Physics Communications **222**, 418 (2018).
[30] X.-D. Xiang, X. Sun, G. Briceo, Y. Lou, K.-A. Wang, H. Chang, W. G. Wallace-Freedman, S.-W. Chen, and P. G. Schultz, A combinatorial approach to materials discovery, Science **268**, 1738 (1995).
[31] A. K., S. J. H. Montoya, J. M. Gregoire, and K. A. Persson, Robust and synthesizable photocatalysts for co$_2$ reduction: a data-driven materials discovery, Nature Communications **443**, 1 (2019).
[32] T. D. Sparks, M. W. Gaultois, A. Olinyk, J. Brgoch, and B. Meredig, Data mining our way to the next generation of thermoelectrics, Scripta Materialia **111**, 10 (2016).
[33] R.-Z. Zhang, F. Gucci, H. Zhu, K. Chen, and M. J. Reece, Data-driven design of ecofriendly thermoelectric high-entropy sulfides, Inorganic Chemistry **57**, 13027 (2018), https://doi.org/10.1021/acs.inorgchem.8b02379.
[34] J. Panand Q. Yan, Data-driven material discovery for photocatalysis: a short review, Journal of Semiconductors **39**, 364 (2018).
[35] G. Hautier, C. Fischer, V. Erlacher, A. Jain, and G. Ceder, Data mined ionic substitutions for the discovery of new compounds, Inorg. Chem. **50**, 656 (2011).
[36] P. Gianozzi, S. Baroni, N. Bonini, M. Calandra, R. Car, C. Cavazzoni, D. Ceresoli, G. L. Chiarotti, M. Cococcioni, I. Dabo, A. D. Corso, S. de Gironcoli, S. Fabris, G. Fratesi, R. Gebauer, U. Gerstmann, C. Gougoussis, A. Kokalj, M. Lazzer, L. Martin-Samos, N. Marzari,

F. Mauri, R. Mazzarello, S. Paolini, A. Pasquarello, L. Paulatto, C. Sbraccia, S. Scandolo, G. Sclauzero, A. P. Seitsonen, A. Smogunov, P. Umari, and R. M. Wentzcovitch, Quantum espresso: a modular and open-source software project for quantum simulations of materials, Journal of Physics: Condensed Matter **21**, 395502 (2017).

[37] P. Gianozzi, O. A. T. Brumme, O. Bunau, M. B. Nardelli, M. Calandra, R. Car, C. Cavazzoni, D. Ceresoli, M. Cococcioni, N. Colonna, I. Carnimeo, A. D. Corso, S. de Gironcoli, P. Delugas, R. D. Jr, A. Ferretti, A. Floris, G. Fratesi, G. Fugallo, R. Gebauer, U. Gerstmann, F. Giustino, T. Gorni, J. Jia, M. Kawamura, H.-Y. Ko, A. Kokalj, E. Kucukbenli, M. Lazzeri, M. Marsili, N. Marari, F. Mauri, N. Nguyen, H.-V. Nguyen, A. O. de-la Roza, L. Paulatto, S. Ponce, D. Rocca, R. Sabatini, B. Santra, M. Schlipf, A. Seitsonen, A. Amogunov, I. Timrov, T. Thonhauser, P. Umari, N. Vast, X. Wu, and S. Baroni, Advanced capabilities for materials modelling with quantum espresso, Journal of Physics: Condensed Matter **29**, 656 (2017).

[38] J. Perdew, A. Ruzsinsky, G. Csonka, O. A. Vydov, G. E. Scuseria, L. A. COnstantin, X. Zhou, and K. Burke, Restoring the density-gradient expansion for exchange in solids and surfaces, Physical Review Letters **100**, 136406 (2009).

[39] G. D. Nguimdoand D. P. Jourbert, A density functional (pbe, pbesol, hse06) study of the structural, electronic and optical properties of the ternary compounds agalx2 (x = s, se, te), European Physical Journal B **88**, 136406 (2014).

[40] M. Benam, N. Abdoshahi, and M. M. Sarmazdeh, Ab initio study of the effect of pressure on the structural and electronic properties of cubic laalo3 by density function theory using gga, lda and pbesol exchange correlation potentials, Physica B **446**, 32 (2014).

[41] M. D. L. Pierre, R. Orlando, L. Maschio, K. Doll, P. uliengo, and R. Dovesi, Performance of six functionals (lda, pbe, pbesol, b3lyp, pbe0, and wc1lyp) in the simulation of vibrational and dielectric properties of crystalline compounds. the case of forsterite mg2sio4, Journal of Computational Chemistry **32**, 1775 (2011).

[42] H. J. Monkhorstand J. D. Pack, Special points for brillouin-zone integrations, Phys. Rev. B **13**, 5188 (1976).

[43] A. D. Corso, Pseudopotentials periodic table: From h to pu, Computational Materials Science **95**, 337 (2014).

[44] F. Tranand P. Blaha, Accurate band gaps of semiconductors and insulators with a semilocal exchange-correlation potential, Phys. Rev. Lett. **102**, 226401 (2009).

[45] P. Blaha, K. Schwarz, F. Tran, R. Laskowski, G. K. H. Madsen, and L. D. Marks, Wien2k: An apw+lo program for calculating the properties of solids, The Journal of Chemical Physics **152**, 074101 (2020), https://doi.org/10.1063/1.5143061.

[46] M. A. Reynoldsand S. N. Milam, Process for producing a copper thiometallate or a selenometallate material (2013), uS Patent 8,409,541.

[47] M. A. Reynolds, Process for producing a thiometallate or a selenometallate material (2015), uS Patent 8,940,268.

[48] C. C. Fischer, K. J. Tibbetts, D. Morgan, and G. Ceder, Predicting crystal structure by merging data mining with quantum mechanics, Nature Materials **5**, 641 (2006).

[49] G. Hautier, C. C. Fischer, A. Jain, T. Mueller, and G. Ceder, Finding natures missing ternary oxide compounds using machine learning and density functional theory, Chemistry of Materials **22**, 3762 (2010), https://doi.org/10.1021/cm100795d.

[50] S. Atahan-Evrenkand A. Aspuru-Guzik, Prediction and calculation of crystal structures, Topics in Current Chemistry **345** (2014).

[51] C. Raymond, P. Dorhout, and S. Miller, Crystal structure of dicaesium tetramolybdate, cs_2mos_4, Zeitschrift fur Kristallographie - Crystalline Materials **210**, 775 (1995).

[52] J. Ellermeier, C. Nather, and W. Bensch, Rb_2mos_4, Acta Crystallographica Section C **55**, 1748 (1995).

[53] M. Emirdag-Eanesand J. A. Ibers, Crystal structure of dipotassium tetrathiomolybdate k_2mos_4, Zeitschrift fur Kristallographie - New Crystal Structures **216**, 484 (2001).

[54] D. Rohnert, C. Nather, and W. Bensch, K_2ws_4, Acta Crystallographica Section C **53**, 165 (1997).

[55] A. Mullerand W. Sievert, Rontgenographische untersuchungen und strukturchemie von chalkogenomolybdaten und wolframaten, Zeitschrift fur Anorganische und Allgemeine Chemie **403**, 251 (1974).

[56] B. R. Srinivasan, C. Näther, A. R. Naik, and W. Bensch, Bis(methylammonium) tetrathiomolybdate(VI), Acta Crystallographica Section E **62**, m1635 (2006).

[57] B. R. Srinivasan, C. Näther, and W. Bensch, Bis(methylammonium) tetrasulfidotungstate(VI), Acta Crystallographica Section E **64**, m296 (2008).

[58] W. Setyawanand S. Curtarolo, High-throughput electronic band structure calculations: Challenges and tools, Computational Materials Science **49**, 299 (2010).

[59] Y. Hinuma, G. Pizzi, Y. Kumagai, F. Oba, and I. Tanaka, Band structure diagram paths based on crystallography, Computational Materials Science **128**, 140 (2017).

[60] R. G. Burns, *Mineralogical Applications of Crystal Field Theory, Second Edition* (Cambridge University Press, 2005) pp. 22–30.

[61] J. Heyd, G. E. Scuseria, and M. Ernzerhof, Hybrid functionals based on a screened coulomb potential, The Journal of Chemical Physics **118**, 8207 (2003), https://doi.org/10.1063/1.1564060.

[62] J. A. Camargo-Martínezand R. Baquero, Performance of the modified becke-johnson potential for semiconductors, Phys. Rev. B **86**, 195106 (2012).

[63] D. J. Singh, Electronic structure calculations with the tran-blaha modified becke-johnson density functional, Physical Review B **82**, 205102 (2010).

[64] H. Jiang, Band gaps from the tran-blaha modified becke-johnson approach: A systematic investigation, The Journal of chemical physics **138**, 134115 (2013).

[65] W. Feng, D. Xiao, Y. Zhang, and Y. Yao, Half-heusler topological insulators: A first-principles study with the tran-blaha modified becke-johnson density functional, Physical Review B **82**, 235121 (2010).

[66] H. Dixit, R. Saniz, S. Cottenier, D. Lamoen, and B. Partoens, Electronic structure of transparent oxides with the tran–blaha modified becke–johnson potential, Journal of Physics: Condensed Matter **24**, 205503 (2012).

[67] D. Waroquiers, A. Lherbier, A. Miglio, M. Stankovski, S. Poncé, M. J. Oliveira, M. Giantomassi, G.-M. Rignanese, and X. Gonze, Band widths and gaps from the tran-blaha functional: Comparison with many-body perturbation theory, Physical Review B **87**, 075121 (2013).

[68] A. D. Beckeand M. R. Roussel, Exchange holes in inhomogeneous systems: A coordinate-space model, Phys. Rev. A **39**, 3761 (1989).

[69] F. Tranand P. Blaha, Importance of the kinetic energy density for band gap calculations in solids with density functional theory, The Journal of Physical Chemistry A **121**, 3318 (2017), pMID: 28402113, https://doi.org/10.1021/acs.jpca.7b02882.

[70] R. A. Jishi, O. B. Ta, and A. A. Sharif, Modeling of lead halide perovskites for photovoltaic applications, The Journal of Physical Chemistry C **118**, 28344 (2014).

[71] B. Traoré, G. Bouder, W. Lafargue-Dit-Hauret, X. Rocquefelte, C. Katan, F. Tran, and M. Kepenekian, Efficient and accurate calculation of band gaps of halide perovskites with the tran-blaha modified becke-johnson potential, Physical Review B **99**, 035139 (2019).

[72] A. France-Lanord, R. Asahi, B. Leblanc, J. Lee, and E. Wimmer, Highly efficient evaluation of diffusion networks in li ionic conductors using a 3d-corrugation descriptor, Scientific Reports **9**, 15123 (2019).